

COMPARISON OF THE EFFECT OF THE APPLIED ENERGY ON THE PROPERTIES OF PROTOTYPES MADE FROM DIFFERENT TYPES OF POWDER MIXTURES

DAVID BRICIN, ANTONIN KRIZ

Department of Material Science and Technology, Faculty of Mechanical Engineering, University of West Bohemia, Pilsen. Czech Republic

DOI: 10.17973/MMSJ.2020_03_2019126

e-mail: bricda@kmm.zcu.cz

The paper deals with the influence of different types of WC-Co powder mixtures processed by SLM technology on the final properties of the prototype build. The powder mixtures used differed in the morphology of the powder particles, i.e. the shape, size and chemical composition of the individual powder particles. In total, two different types of WC-Co powder mixtures were used for the experiment. The study was focused on the evaluation of the effect of these powders and other parameters of SLM technology (applied energy) on the resulting properties of the prototype sample. The samples were subjected to metallographic analysis after their preparation. This analysis was performed using metallographic and scanning electron microscopes. The metallographic analysis was supplemented by analysing the phase composition of the prototype samples and the changes in their chemical composition. The experiments enabled us to compare the differences in the properties of the prototype samples, especially in terms of their porosity, structural changes, changes in chemical and phase composition. The information obtained in relation to the parameters of the technology and the powders provided us with interesting data. The diffusion of the elements, especially carbon, meant the eta phase was formed in all of the samples, which is considered to be an undesirable phase in cemented carbides. However, its volume varied depending on the type of powder and the processing conditions. The smallest amount was recorded for samples made from a powder mixture with a free bond between the binder particles and tungsten carbide grains.

KEYWORDS

SLM technology, WC-Co, cemented carbides, eta phase, porosity

1 INTRODUCTION

WC-Co powder mixtures are used primarily for the production of simple shape components. These are mainly cutting tools, e.g. indexable inserts or drilling heads. These tools have a common means of wear load - abrasion [Sarin 2014]. Pressing or extrusion techniques are used to produce these parts, which results in the desired shape of the part, but which contains a certain percentage of internal porosity. Therefore, the shaping of the component is followed by sintering, which gives the component the final density, mechanical and physical properties [Sarin 2014]; [Upadhyaya 1998]. Using the above processes, it is not possible to create a part with a complex

internal structure providing the required properties. Among the most important is the weight reduction of the component, while maintaining its utility properties or reducing the thermal stress due to the formation of suitably positioned cooling channels. SLM technology can be used to create components with these specific properties. Using SLM technology, the shape of a component is gradually formed in one step and sintered using a continuous filament laser [Gu n.d.]; [Gibson Rosen and Stucker 2015].

SLM technology and its use for processing cemented carbides based on WC-Co are mainly dealt with by research centres.

The published information shows that due to the applied energy, the so-called eta phase M_6C is produced in the prints [Domashenkov 2016]; [Uhlmann 2018]. This phase results in a decrease in the K_{IC} fracture toughness value, a change in hardness and a deterioration in corrosion resistance. The amount and shape of this phase depends on the rate of cooling and the proportion of carbon in the sintered system [García et al. 2019]; [Sarin 2014].

In addition, different porosity levels develop in the prints. The pore types then vary depending on the parameters used to process the powder mixture [Bricin 2018a]; [Uhlmann 2015].

In addition to these changes in the structure of parts made of WC-Co powder mixtures, coarsening and grain shape changes of tungsten carbide occur. These changes are dependent on the process parameters for processing the powder mixture [Gu n.d.]. The WC grain structure can range from elongated to triangular, see Figure 1.

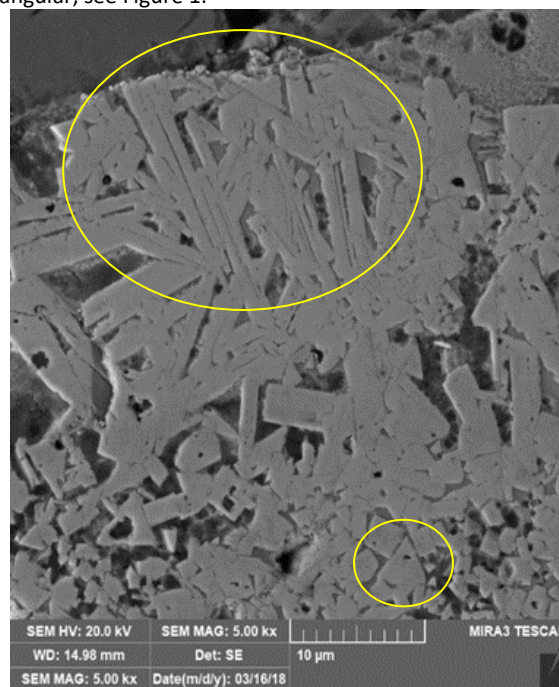


Figure 1. WC-Co print structure magnified 5,000x. The structure shows several WC grain morphologies. The first is grains of rectangular shape (quadrilateral), the second is triangular.

These structural changes, together with the volume of vaporized material, affect the final properties of the prototype part being formed.

The aim of this study is to show, using two types of WC-Co powder mixtures, how the type of powder mixture and its processing parameters influence the final properties of the prototype part being created. For this reason, the same volume energy density was used to produce prototype sample $E_v = 238 \text{ J/mm}^3$, see equation 1 [Uhlmann 2015]; [AlMangour n.d.]; [Srivatsan n.d.].

$$E_v = (P / (l_s \cdot h_s \cdot v_s)) \text{ [J/mm}^3\text{]} \quad (1)$$

The parameters used to process the powder blends then varied in the laser power used, the laser spot scanning rate, and the thickness of the powder layer formed. As a result, it was possible to achieve different types of porosity, different changes in their structure and ultimately in their resulting mechanical properties.

2 EXPERIMENTAL MATERIAL AND METHODS

Two types of WC-Co powder mixtures were used as experimental material. The first mixture was obtained by processing CTE50DF powder blend (trade name) to remove the secondary binder from the powder mixture so the only bonds between the tungsten carbide particles and the Co binder were weak physical forces, see Fig. 2.

The authors of the article have already published several case studies concerning its processability and applicability for the SLM process. [Bricin 2018a]; [Bricin 2018b]; [Bricin 2018c]. The average particle size of this powder mixture was about $240 \pm 74 \mu\text{m}$.

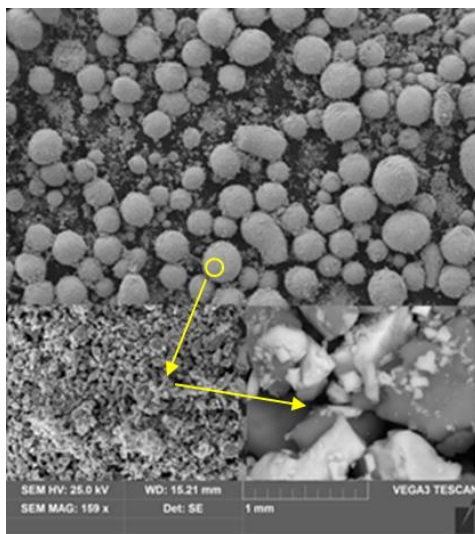


Figure 2. Structure of CTE50DF powder particle mixture. The image contains a detail of the structure. It can be seen that cobalt particles (dark grey particles) and tungsten carbide grains (light-white particles) are not bound to each other, for example by a secondary type of binder

The second powder mixture used in this experiment was the AW701 powder mixture in which the tungsten carbide particles were bound with a binder in the form of granules, see Fig. 3. The average size of these granules, of the powder particles, was around $30 \pm 8.1 \mu\text{m}$.

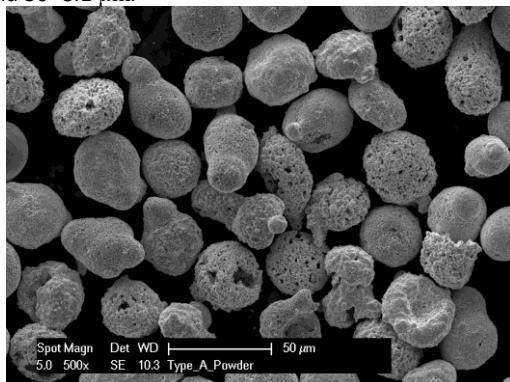


Figure 3. Structure of AW701 powder mixture particles. It can be seen from the figure that the surfaces of the powder particles have surface defects. These defects include cavities and craters

Both of the powder mixtures were analysed for phase composition, see Fig. 4, which showed that the powder

mixtures consisted of Co binder and tungsten carbide WC grains. In the case of the second powder mixture (AW701), the phase $\text{W}_{0.2}\text{Co}_{0.8}$ was also identified. This phase originated due to the technology used for its production.

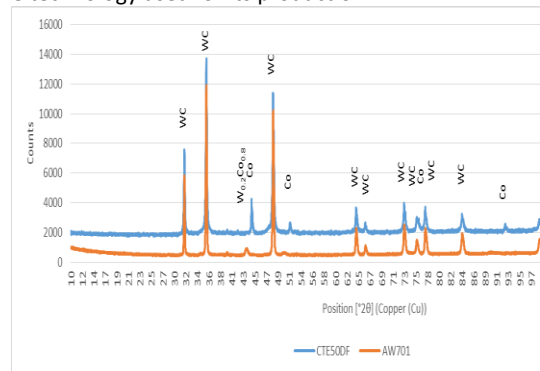


Figure 4. Phase composition of powder mixtures used for production of prototype samples

In addition to the difference in phase composition, the powder blends differed in the initial chemical composition and in the tungsten carbide grain size. The CTE50DF powder blend contained a larger weight fraction of binder (25 wt%). The AW701 powder blend contained only 12 wt. % binder. As a result, this mixture was more likely to develop cracks in the prototype sample structure. The probability of cracking increases with a decreasing proportion of binder in the structure of the prototype samples [Khmyrov 2016]. For the CTE50DF powder mixture, the average grain size of the tungsten carbide WC was around $6 \pm 2 \mu\text{m}$. In the AW701 powder mix, the grain size value was around $3 \pm 2 \mu\text{m}$.

Prototype samples were made from both powder mixtures on an additive SLM device. The same value of applied bulk energy density was used to produce prototype samples ($E_v = 238 \text{ J/mm}^3$). The other processing parameters of the powder mixtures are shown in Table 1.

Powder mixture	Laser power P (W)	Scan speed (mm/s)	Layer thickness (mm)
CTE50DF	280	100	0,1
AW701	40	35	0,04
	80	70	0,04
	100	87.5	0,04

Table 1. Process parameters used for WC-Co powder mixtures

Prototype samples in the form of 10mm cubes were created using these parameters, see Fig. 5.



Figure 5. Printed samples from AW701 powder mix

After their production, they underwent metallographic analysis. This analysis consisted of the preparation of a metallographic cut and subsequent evaluation of the sample structure using an Observer Z1m Carl Zeiss metallographic microscope, Tescan Mira3 scanning electron microscope and Philips XL30ESEM scanning electron microscope. The sample structure was visualized by chemical etching according to ASTM B657

[18_2019]. Changes in the chemical composition of the samples were recorded using an EDX chemical composition analyser. After metallographic analysis of the structure of the samples, their phase composition was analysed. This analysis was performed on a PANalytical X'Pert PRO X-ray diffractometer, using the Bragg-Brentano method, using a $\text{CuK}\alpha$ X-ray source.

3 EXPERIMENTAL RESULTS AND DISCUSSION

The first analysis performed on the printed samples was the analysis of their density, see Fig. 6. The graph shows that the final print density is influenced by the value of the laser power; using a higher laser power increases the density of the printed sample. The graph also shows that a prototype sample made from CTE50DF powder blend achieved a lower density value despite the use of higher laser power (280 W). This was associated with the type of powder mixture used, where the particle size of the powder caused problems with proper powder application. [Bricin 2018a]. As a result, an uneven powder layer was formed which led to an increase in the porosity of the printout.

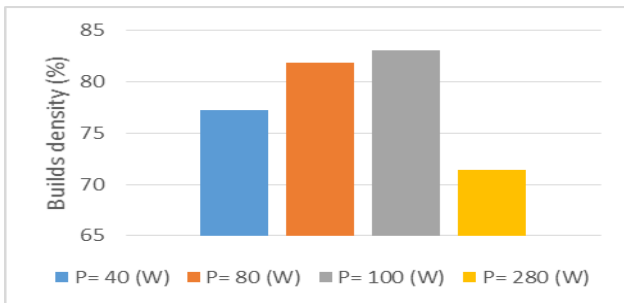


Figure 6. Comparison of density of printed samples from CTE50DF and AW701 powder mixture

The particle size of the powder also necessitated the use of a greater thickness of the applied powder layer. This also increased the porosity of the CTE50DF powder print. The influence of the thickness of the powder layer on the density of the printed samples is confirmed by previously published articles [Qiu 2019]; [Wei and Du, 2019]; [Sufiiarov 2019]; [Uhlmann 2015]. In the case of a greater thickness of the applied powder layer, the size of the temperature field formed may not be large enough. As a result, the material does not need to melt throughout the required volume despite the use of higher applied power value. This has also been demonstrated in the CTE50DF powder mixture print. This may result in an imperfect connection of the sintered powder lines or powder particles in the powder bed. This leads to an increase in the porosity of the printed sample.

The processing parameters of the powder mixture affect the pore structure and their final size in the structure of the build. The graphs in figures 7 and 8 show how the laser power affects the shape and pore size of the structure of the build.

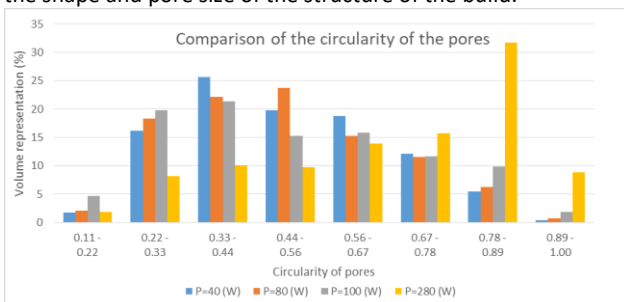


Figure 7. Comparison of pore shape changes in the structure of printed

samples from AW701 and CTE50DF powder mixture

It can be seen from Fig. 7 that the increase in applied power results in more pronounced pore formation with a circular cross-section. The pores formed are then smaller in size, see Fig. 8.

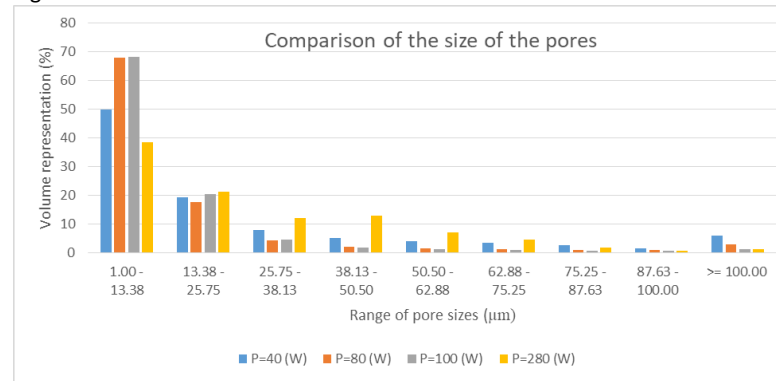


Figure 8. Comparison of pore size changes in the structure of printed samples from AW701 and CTE50DF powder mix

From Fig. 8 it can be seen that the pore size of the sample printed from the CTE50DF powder mixture contains a larger pore size of 25-75 microns than the AW701 powder mixture prints. This is associated with the larger layer thickness in which the powder is applied to the building plate of the additive device. Comparing the pore sizes of the samples printed from the AW701 powder blend, it can be seen that the pore size is gradually reduced. This, in turn, results in a reduction in the proportion of open, interconnected pores in the structure of the printed samples, which in turn affects the possibility of further processing of the samples by infiltration or the HIP process. While processing the powder mixtures, it was also possible to observe flying particles from the point of interaction of the laser beam with the powder mixture. These particles could then be found on the surface of the printed samples or in their volume, see Fig. 9.

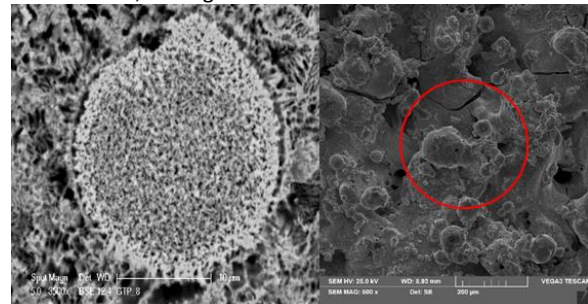


Figure 9. The left part of the figure shows a departed particle trapped in the volume of the printed sample. The right part of the figure shows the balling effect of particles on the printed sample surface

The formation of these particles is associated with a phenomenon known as the "Balling Effect". As mentioned in previously published articles, the intensity of this phenomenon is dependent on the chemical composition of the powder particles, their rheological and physical properties, and the process parameters used for these powder mixtures. [Zhou et al 2015]; [Gu and Shen 2009]; [Tolochko et al. 2004]. The process parameters and the properties of the processed powder mixtures further influence the volume of the vaporized material, see Fig. 10.

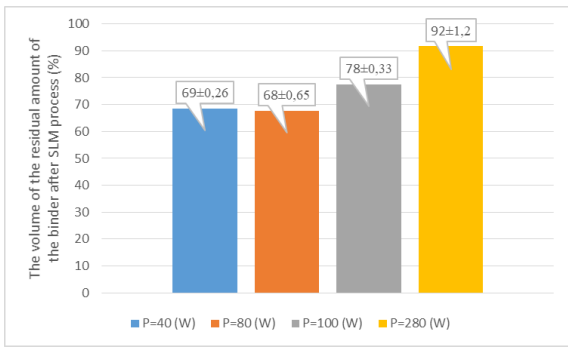


Figure 10 Comparison of binder loss when changing the applied laser power

From Figure 10 it can be seen that at the same applied energy density value, the vaporized binder volume was lower when using higher laser power. This can be explained by the fact that the higher the laser power, the higher the temperature reached in the powder bed volume. However, due to the use of a higher laser spot scanning rate, the vaporization time of the components of the sintered system is shortened. It also follows that, in addition to the applied power, the volume of vaporized material is primarily dependent on the speed at which the laser spot moves.

X-ray diffraction analysis of the phase composition on the printed samples showed that the processing of the powder mixtures caused the so-called $\text{Co}_3\text{W}_3\text{C}$ phase precipitates in their volume, see fig. 11.

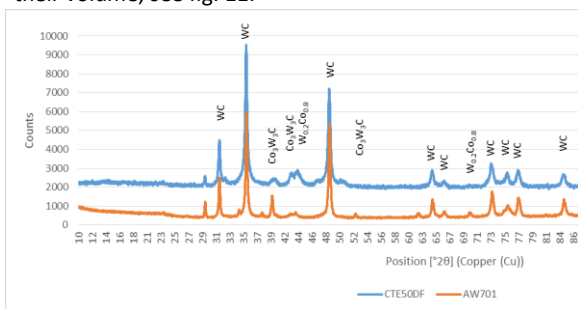


Figure 11. Phase composition of created prototype samples from powder mixtures CTE50DF and AW701

This phase precipitated due to the fact that the Co binder melts during the powder mixture processing. Since cobalt as a binder is mutually soluble with both carbon and tungsten, these interstitial and substitution elements are diffused into the molten binder at sufficiently high temperatures in the presence of the melt. Subsequent rapid cooling, which is due to the dynamics of the SLM powder blend process, leads to the formation of (precipitation) of the eta phase. This phase is, for example, undesirable in terms of fracture toughness of SK products because it reduces its value.

The metallographic analysis revealed that the newly precipitated phase does not occur in the entire volume of the printed samples, see figures 12 and 13.

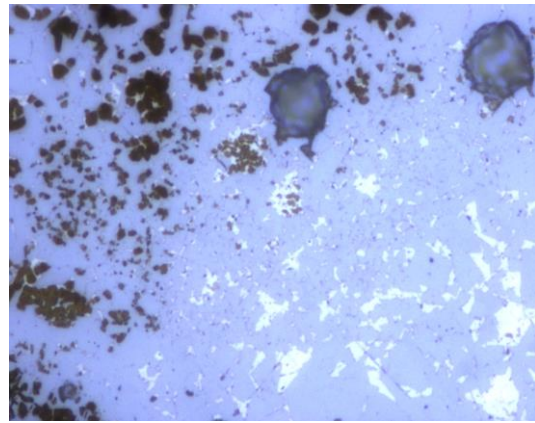


Figure 12. Structure of print made from the AW701 powder mixture. Tungsten carbide grains (grey formations), Co binder (white areas), eta phase (orange-brown formations) and pores of the circular cross-section are shown.

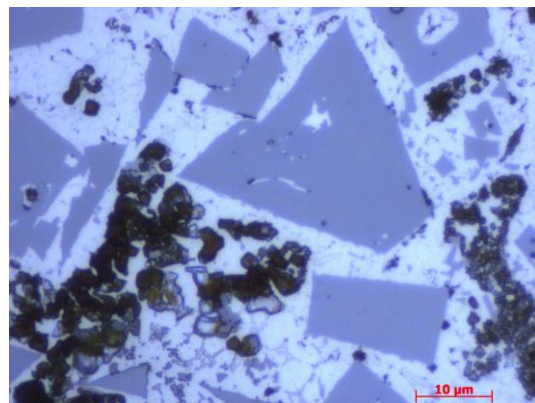


Figure 13. Structure of print made from powder mixture CTE50DF. Tungsten carbide grains (grey formations), Co binder (white areas), and eta phase (orange-brown formations) are seen.

From figures 12 and 13 it can be seen that the structure of the printed samples was largely heterogeneous after production. The mixing of the individual phases was largely dependent on the Marangoni effect, which is also involved in the formation of the Balling effect mentioned earlier.

The Marangoni effect results in a lowering of the temperature gradient in the molten region of the powder bed, which contributes to the intermixing of the solid phase and molten binder and thus also affects the final density of the future print. [Kruth et al. 2007].

The intensity of the final mixing of the structural phases as published in previous research is dependent on the applied laser power and the speed of laser spot motion [Wang et al. 2016]; [Bricin 2018a].

In addition to the above, tungsten carbide grains were significantly coarsened. Grain size increases of up to 200% were observed with AW701 powder blends. The CTE50DF powder mixture also markedly coarsened the WC grains by approximately the same value as was found for powder blend AW701.

All of the changes described above which occurred during the processing of the powder blend result in a change in the mechanical and physical properties of the printed prototype samples.

4 CONCLUSION

The aim of this experimental study was to compare the properties of prototype samples that were printed at the same applied energy density $E_v = 238 \text{ J/mm}^3$, but at different laser power and scan rate parameters, from two different types of WC-Co powder mixtures.

Metallographic analysis and X-ray diffraction analysis revealed that:

- Due to the powder blending process, the $\text{Co}_3\text{W}_3\text{C}$ phase is precipitated in the print structure.
- The distribution of the structural phases - their mixing- was dependent on the Marangoni effect, which is mainly known from welding and surfacing processes of materials.
- The volume of vaporized binder or material, in addition to the applied power, was dependent on the speed of movement of the laser spot used. For samples printed using a higher laser power, a reduced evaporation loss was observed, and this was aided by the use of a higher scanning speed that was used to achieve the same applied energy density E_v .
- The applied laser power largely influenced the final shape and pore size. The higher power of the laser spot resulted in a larger melt volume, causing an increase in the number of PCBs between the powder particles in the powder bed. This resulted in a gradual closure of the pores and a transition from the open pore structure to the closed pore structure and an increase in the density of the printed prototype samples.

The results of the above analyses will be supplemented in future research with the results of analyses that investigate the effect of WC-Co powder treatment parameters on their mechanical properties and corrosion resistance. In addition, further research into the additive processing of WC-Co powder blends will focus on technology operations that would be able to enhance the utility properties of a printed prototype sample. These will be primarily heat treatment technologies, infiltration and omnidirectional heat treatment techniques known as HIP.

ACKNOWLEDGEMENT

The paper was based on the solution of the student project SGS - 2018-051 "Application of new methods of surface treatment and testing of materials and materials in order to increase the applicability of a component or work tool in industrial practice". The authors also thank Michal Ackermann and Jiří Šafka from the Technical University of Liberec for using their laboratory of additive techniques to produce samples made of WC-Co powders.

REFERENCES

[18 2019] 18, A. (2019). ASTM B657 - 18 Standard Guide for Metallographic Identification of Microstructure in Cemented Carbides. [online] Astm.org. Available at: <https://www.astm.org/Standards/B657.htm> [Accessed 2 Oct. 2019].

[AlMangour n.d.] AlMangour, B. (n.d.). Additive manufacturing of emerging materials.

[Bricin 2018a] Bricin, D., Spirit, Z. and Kriz, A. (2018). Metallographic Analysis of the Suitability of a WC-Co Powder Blend for Selective Laser Melting Technology.

[Bricin 2018b] Bricin, D. and Kriz, A. (2018). Assessment of Usability of WC-Co Powder Mixtures for SLM. *Manufacturing Technology*, 18(5), pp.719-726.

[Bricin 2018c] Bricin, D., Kriz, A. (2018). Comparison of Metallography and Mechanical Properties of Samples Printed from WC-Co Powder Mix Using SLM Technology in Protective Atmospheres of Argon and Nitrogen. *Materials, Methods & Technologies*. Volume 12. pp. 326-334.

[Domashenkov 2016] Domashenkov, A., Borbely, A. and Smurov, I. (2016). Structural modifications of WC/Co nanophased and conventional powders processed by selective laser melting. *Materials and Manufacturing Processes*, 32(1), pp. 93-100.

[García et al. 2019] García, J., Collado Ciprés, V., Blomqvist, A. and Kaplan, B. (2019). Cemented carbide microstructures: a review. *International Journal of Refractory Metals and Hard Materials*, 80, pp.40-68.

[Gibson Rosen and Stucker 2015] Gibson, I., Rosen, D. and Stucker, B. (2015). *Additive manufacturing technologies*. New York, NY: Springer.

[Gu and Shen 2009] Gu, D. and Shen, Y. (2009). Balling phenomena in direct laser sintering of stainless steel powder: Metallurgical mechanisms and control methods. *Materials & Design*, 30(8), pp.2903-2910.

[Gu n.d.] Gu, D. (n.d.). *Laser Additive Manufacturing of High-Performance Materials*.

[Khmyrov 2016] Khmyrov, R., Safronov, V. and Gusarov, A. (2016). Obtaining Crack-free WC-Co Alloys by Selective Laser Melting. *Physics Procedia*, 83, pp.874-881.

[Kruth et al. 2007] Kruth, J., Levy, G., Klocke, F. and Childs, T. (2007). Consolidation phenomena in laser and powder-bed based layered manufacturing. *CIRP Annals*, 56(2), pp.730-759.

[Qiu 2019] Qiu, C., Panwisawas, C., Ward, M., Basoalto, H., Brooks, J. and Attallah, M. (2019). On the role of melt flow into the surface structure and porosity development during selective laser melting. [online] Mendeley. Available at: <https://www.mendeley.com/catalogue/role-melt-flow-surface-structure-porosity-development-during-selective-laser-melting/> [Accessed 14 Oct. 2019].

[Sarin 2014] Sarin, V. (2014). *Comprehensive Hard Materials*. Elsevier.

[Srivatsan n.d.] Srivatsan, T. and Sudarshan, T. (n.d.). *Additive manufacturing*.

[Sufiiarov 2019] Sufiiarov, V., Popovich, A., Borisov, E., Polozov, I., Masaylo, D. and Orlov, A. (2019). The Effect of Layer Thickness at Selective Laser Melting. [online] Mendeley. Available at: <https://www.mendeley.com/catalogue/effect-layer-thickness-selective-laser-melting/> [Accessed 14 Oct. 2019].

[Tolochko et al. 2004] Tolochko, N., Mozzharov, S., Yadroitsev, I., Laoui, T., Froyen, L., Titov, V. and Ignatiev, M. (2004). Balling processes during selective laser treatment of powders. *Rapid Prototyping Journal*, 10(2), pp.78-87.

[Uhlmann 2015] Uhlmann, E., Bergmann, A. and Gridin, W. (2015). Investigation on Additive Manufacturing of Tungsten Carbide-cobalt by Selective Laser Melting. *Procedia CIRP*, 35, pp.8-15.

[Upadhyaya 1998] Upadhyaya, G. (1998). *Cemented tungsten carbides*. Westwood, N.J.: Noyes Publications.

[Wang et al. 2016] Wang, L., Jue, J., Xia, M., Guo, L., Yan, B. and Gu, D. (2016). Effect of the Thermodynamic Behavior of Selective Laser Melting on the Formation of In situ Oxide Dispersion-Strengthened Aluminum-Based Composites. *Metals*, 6(11), p.286.

[Wei and Du 2019] Wei, Z. and Du, J. (2019). Heat and Mass Transfer of Additive Manufacturing Processes for Metals. [online] Intechopen.com. Available at: <https://www.intechopen.com/online-first/heat-and-mass->

transfer-of-additive-manufacturing-processes-for-metals

[Accessed 14 Oct. 2019].

[\[Zhou et al 2015\]](#) Zhou, X., Liu, X., Zhang, D., Shen, Z. and Liu, W. (2015). Balling phenomena in selective laser melted tungsten. *Journal of Materials Processing Technology*, 222, pp.33-42.

CONTACTS:

Ing. David Bricin
University of West Bohemia in Pilsen
Univerzitni 22
306 14 Plzen
Tel: +420 377 638 314
e-mail: bricda@kmm.zcu.cz